Science of the Total Environment 854 (2023) 158754

Contents lists available at ScienceDirect

Science of the Total Environment

journal homepage: www.elsevier.com/locate/scitotenv

Arsenate removal using titanium dioxide-doped cementitious composites: Mixture design, mechanisms, and simulated sewer application

Zhuo Liu [a], Qiantao Shi [a,b,*], Yi Bao [a], Xiaoguang Meng [a,b], Weina Meng [a]

[a] Department of Civil, Environmental and Ocean Engineering, Stevens Institute of Technology, 1 Castle Terrace Point, Hoboken, NJ 07030, USA
[b] Center for Environmental Systems, Stevens Institute of Technology, 1 Castle Terrace Point, Hoboken, NJ 07030, USA

HIGHLIGHTS

- A novel TiO_2-doped cementitious composite (TCC) was fabricated for As(V) removal.
- Ratios of TiO_2-to-cement and water-to-cement are the dominant factors in As(V) removal.
- A sewer made of TCC was set up and decontaminated As(V) from the following water.
- Both precipitations with calcium and adsorption on TiO_2 contribute to As(V) removal.
- Adsorption of As(V) on TiO_2 is more significant at lower As concentration.

GRAPHICAL ABSTRACT

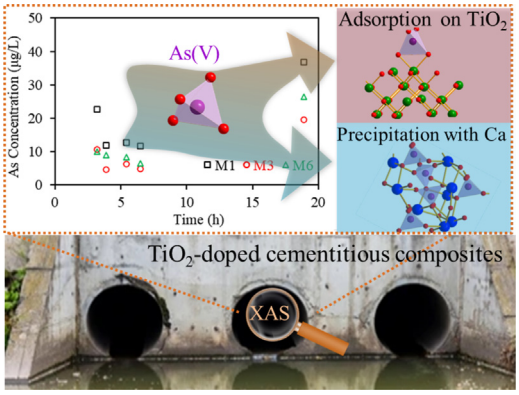

ARTICLE INFO

Editor: Xinbin Feng

Keywords:
Arsenate
Cementitious composite
TiO_2
Adsorption
Precipitation

ABSTRACT

Arsenate (As(V)) in municipal wastewater leads to a public health problem due to its contamination of natural water sources. Here, we proposed to use sewer pipe made of TiO_2-doped cementitious composite (TCC) for As(V) removal from municipal wastewater. The optimum composition of TCC, the performance for As(V) removal in the simulated sewer system, and the molecular-level As(V) removal mechanisms were investigated. To obtain the optimum composition, variables were adjusted to maximize the As(V) removal using TCC. Results show that the TiO_2 and water contents were the dominant factors. Simulated sewer pipes made of TCC removed As(V) from 100 μg/L to <10 μg/L, which performed better than plain cementitious composite. Moreover, extended X-ray absorption fine structure (EXAFS) analysis indicates that both precipitation and adsorption contribute to the As(V) removal by TCC, while the adsorption is more significant with a lower As(V) concentration (i.e., 1 mg/L). This is the first study evaluating the feasibility to apply TCC for As(V) removal from sewer wastewater. The optimized composition, simulation results, and molecular-level mechanism gained from this study are useful to the future design of TCC for As(V) removal, especially for sewer systems.

1. Introduction

Arsenic (As) contamination has attracted intensive attention due to its worldwide presence and high toxicity (Abdul et al., 2015; Pena et al., 2005). About 94 to 220 million people were exposed to water with high As concentrations (Podgorski and Berg, 2020). The problem is more serious in

* Corresponding author at: Department of Civil, Environmental and Ocean Engineering, Stevens Institute of Technology, 1 Castle Terrace Point, Hoboken, NJ 07030, USA.
E-mail address: qshi4@stevens.edu (Q. Shi).

http://dx.doi.org/10.1016/j.scitotenv.2022.158754
Received 17 July 2022; Received in revised form 30 August 2022; Accepted 9 September 2022
Available online 13 September 2022

developing countries, such as Bangladesh, India, Vietnam, Chile, Iran, and China (Amini et al., 2008; Brammer and Ravenscroft, 2009; Eslami et al., 2022), and also about 2.1 million people in the United States are affected by As-contaminated water (Ayotte et al., 2017). As is a naturally occurring element in groundwater but also exists at high levels in many other water systems because of anthropogenic activities, e.g., mining, smelting, glass manufacturing, and agricultural process (Andrianisa et al., 2008; Singh et al., 2015).

Arsenic (As) has been detected in different types of municipal wastewater and mainly exist as arsenate (As(V), accounts for 41.7–74.3 % of the total As) (Zhai et al., 2020), which endangers human health. However, while numerous studies have been reported regarding the As(V) removal from groundwater and mining wastewater, there are limited reports on As(V) removal from municipal wastewater. Hence, this study proposes to remove As(V) using a sewage pipe fabricated with a cementitious composite. This method is expected to be convenient to implement in the existing sewer systems and capable of significantly reducing As(V) from municipal wastewater.

To achieve this goal, a cementitious composite with high efficacy of As(V) removal. It was already reported that cement can remove As(V) from water (Kundu et al., 2004). Moreover, iron oxides were used to modify cement to improve its efficacy (Kundu and Gupta, 2006a), because of the high As(V) removal ability of iron-based materials (Eslami et al., 2019; Eslami et al., 2018; Eslami et al., 2020). Nevertheless, the removal mechanisms were not clarified in these studies, which limits the understanding and further improvement of this kind of adsorbent. Meanwhile, nano-TiO_2 and nano-TiO_2-based materials were widely used to remove inorganic and organic As(V) with high efficacies (Pena et al., 2005; Jing et al., 2005; Bang et al., 2011). Therefore, it is envisioned that a type of TiO_2-doped cementitious composite (TCC) is a promising adsorbent to remove As(V) from sewage systems.

However, it remains unclear how the combination of concrete and TiO_2 particles performs in As removal. It is also unknown whether TiO_2-doped concrete will gain desired performance in As(V) removal from municipal wastewater while retaining desired mechanical properties. This research aims to evaluate the effects of concrete doped with TiO_2 nanoparticles on the performance of As(V) removal and its mechanical properties, as well as understand the underlying mechanisms. Specifically, there are three main objectives: (1) The effects of mixture design variables of TCC on the As(V) removal performance and the mechanical properties are evaluated, and the underlying mechanisms of the changes of mechanical properties are investigated. (2) The As(V) removal mechanisms by TCC, i.e., distinguishing the adsorption and precipitation. (3) The performance of TCC in removing As(V) from municipal wastewater in a simulated sewage pipe under a flowing condition.

In this study, to achieve these objectives, a total of nine cementitious composite mixtures were designed and tested. The mechanical properties and the hydration kinetics of TCC were investigated. Then, the As(V) removal performance was evaluated in different aspects: (1) The As(V) removal efficacy was evaluated by the single-point test, kinetic test, and isotherm test. (2) The effects of coexisting anions and reusability of TCC were tested. (3) The performance of TCC in a simulated sewer system made using TCC was tested as a potential use case. Finally, to elucidate the mechanisms, the pore structure of TCC was evaluated by mercury intrusion porosimetry (MIP) and its relationship with As(V) adsorption was analyzed, and the adsorption configuration and possible precipitation were identified by X-ray absorption spectroscopy (XAS). Overall, this study evaluates the feasibility to apply TCC for As(V) removal in a sewer system by evaluating the As removal performance at different scales and exploring the microstructural and molecular-level mechanisms of As(V) removal.

2. Materials and methods

2.1. Preparation of cementitious composite

TCC was prepared with Type I Portland cement, river sand (Whibco of New Jersey, USA), tap water, high-range water reducer (BASF MasterGlenium® 7620, USA), and nano-TiO_2 particles (Aeroxide® P25, Evonik, USA). The chemical properties of the tap water used in this study are shown in Table S1 in the Supplementary data. The chemical composition and the specific gravity of the cement are shown in Table S2. The particle size distribution of the river sand is shown in Fig. S1. The main characteristics of the nano-TiO_2 particles are shown in Table S3. The morphology of the nano-TiO_2 particles observed by Scanning electron microscopy (SEM) is shown in Fig. S2. A polycarboxylate-based high-range water reducer (HRWR) was used to improve the flowability of the mixtures.

For the mixture design, four variables were investigated, namely, TiO_2-to-cement ratio (Ti/c), water-to-cement ratio (w/c), sand-to-cement ratio (s/c), and lightweight sand content (LWS). These four variables were selected because (1) The nano-TiO_2 content directly affects the As(V) adsorption performance; (2) Ti/c, w/c, s/c, and LWS are the factors affecting the composition and the microstructures of cementitious composites, which in turn affect the mechanical properties and As(V) adsorption of TCC.

Nine mixtures were investigated (Table 1): Mixture 1 (M1) was a plain cementitious composite without nano-TiO_2, which was tested as the control. Mixtures M2, M3, and M4 had different Ti/c. According to preliminary tests, mixtures with different w/c (M5 and M6), s/c (M7 and M8), and LWS content (M9) were prepared with a fixed Ti/c of 0.05.

A 5-L mixer (Hobart N50 mixer) was used to fabricate the mixtures in four steps: (1) mix ingredients and sand at 60 rpm for 90 s; (2) add 80 % of the required amount of water and mix at 120 rpm for 120 s; (3) add the rest 20 % of water and mix at 120 rpm for 60 s; (4) scrap the mixer and mix for another 60 s. The temperature was controlled at 20 °C.

Cubic specimens with a side length of 50 mm were cast in molds and placed on a vibrating table. Immediately after casting, the specimens were covered by wet burlap and a plastic sheet. The cubic specimens were demolded after 1 d and then cured in lime-saturated water at room temperature (23 ± 2 °C) until the age of testing.

2.2. Properties of cementitious composites

The rate and extent of hydration were evaluated using an isothermal calorimeter (Calmetrix I-Cal 4000 HPC). About 60 g of fresh suspension was sealed in a plastic vial and placed into the calorimeter at 25 °C. The heat of hydration was continuously measured from 2 min after mixing and continued to 48 h. The results were normalized by the mass of the binder.

The compressive strength of these samples was measured after 1 d, 7 d, and 28 d of standard curing using 50-mm cubes with a loading rate of 1.8 kN/min, according to ASTM C109 (Standard Test Method for Compressive Strength of Hydraulic Cement Mortars).

The phases in the hardened cementitious composite were evaluated using a thermal analyzer (model: TA® TG55). Around 20 mg of dried powder crushed from cubic samples were tested. The temperature was programmed from 20 to 1000 °C at a speed of 10 °C/min with a 30 mL/min flow of nitrogen gas.

Table 1
The mass ratios in the investigated mixtures.

Designation	Cement	Water	River sand	LWS	Nano-TiO_2	Water reducer	Note
M1	1	0.4	1	0	0	0.005	Control
M2	1	0.4	1	0	0.025	0.005	Ti/c
M3	1	0.4	1	0	0.05	0.005	
M4	1	0.4	1	0	0.1	0.005	
M5	1	0.2	1	0	0.05	0.005	w/c
M6	1	0.6	1	0	0.05	0.005	
M7	1	0.4	0.5	0	0.05	0.005	s/c
M8	1	0.4	1.5	0	0.05	0.005	
M9	1	0.4	0.5	0.34	0.05	0.005	LWS

2.3. Adsorption tests

Batch adsorption experiments including single-point, kinetics, and isotherms were conducted to evaluate the adsorption efficacy of the cementitious composite adsorbents. For the batch experiment, the mixture was ground into powders as adsorbent and then mixed with As(V) solutions on a rotator at 30 rpm for the designed time. Then the solutions were centrifugated at 9000 rpm for 10 min, separated, and acidified using HNO_3. Finally, the As concentrations were measured by graphite furnace atomic absorption spectrometry (GFAAS, Agilent Z240, U.S.).

For the single-point test, 0.05 g mixture was added into a 50 mL 1 mg/L As(V) solution and mixed for 24 h. The As(V) solution was prepared by diluting the 1 g/L As(V) stock solution using tap water, and the pH was maintained at 6.8–7.2. Triplicate tests were conducted.

Three mixtures were selected based on the single-point test for further kinetic and isotherm studies. According to the preliminary tests, the kinetics was conducted by mixing 10 g/L mixtures with 1 mg/L As(V) solution. Samples were taken at the designated time, i.e., after mixing for 10 min, 30 min, 1 h, 2 h, 4 h, 8 h, 16 h, 24 h, 36 h, 48 h, and 72 h. For the isotherm study, 0.2–20 g/L mixtures were mixed with 1 mg/L As(V) for 72 h to investigate the As(V) removal ability of these three selected mixtures. For all batch tests, the final pH of the As(V) solutions was within 6.8–7.2.

2.4. Effects of the presence of coexisting anions

To investigate the possible competitive effects of coexisting anions, As(V) removal tests on mixtures M1, M3, and M6 were conducted in the absence and presence of phosphate (PO_4^{3-}), sulfate (SO_4^{2-}), bicarbonate (HCO_3^-), or silicate (SiO_3^{2-}). The concentrations of As(V) and these coexisting ions were all 1 mg/L, while the concentrations of M1, M3, and M6 were all 1 g/L. The mixing time was 72 h. Triplicate tests were conducted.

2.5. Reusability test

To evaluate the reusability of TCC for As(V) removal, the TCC used in the batch tests was regenerated by the NaOH solution and reused for three cycles. Specifically, the solid mixture after As(V) adsorption was separated by centrifugation and mixed with 10 mL 1 M NaOH for 1 h. Then, the solid was separated from NaOH and washed with 20 mL DI water three times for reuse.

2.6. Simulated sewer test

To simulate a sewer system, a small-scale flowing channel (Fig. S3) was designed to investigate the efficacy of the proposed TCC on As(V) removal. The simulated sewer system is an opening channel with a length of 1 m, a slope of 1/50 (height/length), and a cross-section of 25.4 × 25.4 mm. During the experiment, the solution of 100 μg/L As(V) was pumped using a peristaltic pump into the channel at a flow rate of 1 mL/min. Samples at the end of the channel were collected five times per day in the first 2 d, and then twice per day until the breakthrough.

2.7. Characterizations

The porosity and pore size distribution of the samples were determined using mercury intrusion porosimetry (MIP) (Anton Paar Poremaster, USA). For each investigated mixture, about 1 g of samples with the size of 5 mm × 5 mm × 5 mm were tested. The applied pressures ranged from 0.1 to 400 MPa.

The morphology of TCC M3 was investigated by SEM (Zeiss Auriga FIB/SEM, USA). The distribution of the Ti was captured by energy-dispersive X-ray spectroscopy (EDS) mapping. Cubic samples with the size of 20 × 20 × 20 mm were cut from the cubic specimens using a concrete saw at 28 d. The samples were vacuum-dried and then embedded in epoxy resin. The samples were hardened and polished with silicon carbide papers. Results in Fig. S4 show that Ti element distributes evenly in the TCC, implying that nano-TiO_2 particles are uniformly dispersed.

To study the precipitation and adsorption of As(V) on TCC, As K-edge (11,867 eV) XAS was collected at beamline 9-BM at the Advanced Photon Source (Argonne National Laboratory, United States). An energy range of −200 eV to 14 *k* relative to the As K-edge was used to acquire spectra in fluorescence mode with a 4-element vortex silicon-drift detector or transmission mode according to the adsorbed amount of As on these samples. Thirteen scans were collected for each sample and averaged to improve the signal/noise ratio. The spectra were first processed by ATHENA and then simulated using a FEFF shell-by-shell fitting using ARTEMIS (Newville, 2001; Ravel and Newville, 2005), in line with our previous studies (Zhang et al., 2020; Shi et al., 2020), and the details are described in Text S1.

3. Results and discussion

3.1. Mechanic properties of TCC

The rate of heat evolution for the cementitious composites of M1 (Ti/c = 0), M2 (Ti/c = 0.025), M3 (Ti/c = 0.05) and M4 (Ti/c = 0.1) were investigated by the heat flow (Fig. 1A). Results indicate that the maximum heat flow (peak) of M2 (7 h), M3 (6 h), and M4 (5 h) occurred earlier than that of M1 (12 h). Also, the intensities of heat flow for M2 (9.8 mw/g), M3 (10.8 mw/g), and M4 (11.8 mw/g) were higher than that for M1 (7.2 mw/g). The peak of the heat flow results from cement hydration (Zhenhai et al., 2017). Hence, the results imply that the increase of Ti/c accelerated cement hydration. The acceleration of cement hydration leads to more hydration products, enhances the mechanical properties, and densifies the microstructures of TCC.

Similarly, TCC (M2, M3, and M4) released more cumulative heat in the first 10 h than M1 (Fig. 1B). M2 released the highest cumulative heat among these four materials. The released heat from cementitious composite comes from cement hydration. In this case, M2 has a lower cement content (41 %) than M1 (42%), but released higher heat, because the grain boundary region was densely populated and transformed completely early in the presence of TiO_2 nanoparticles (Chen et al., 2012). Among these three TCC materials, M3 and M4 showed lower cumulative hydration heat than M2, because of their lower cement content (40 % and 39 % for M3 and M4, respectively) and agglomeration of nano-TiO_2 (Jiang et al., 2021).

The compressive strength of these four mixtures is presented in Fig. 1C. As expected, the compressive strengths of M2 (71 MPa), M3 (66 MPa), and M4 (64 MPa) at the curing age of 28 d were significantly higher than that of M1 (55 MPa). However, although M3 and M4 had higher Ti/c (0.05–0.1) than M2 (0.025), the compressive strengths of M3 and M4 were lower than that of M2, agreed well with the hydration kinetic results (Fig. 1-A and B).

The hydration products of M1, M2, M3, and M4 are analyzed by the thermogravimetric analysis (TGA, Fig. 2-A and B). The contents of bonded water and $Ca(OH)_2$ were determined as the weight loss at 105–400 °C (Fig. 2-C) and 400–500 °C (Fig. 2-D), respectively (Qin et al., 2018). Overall, the incorporation of nano-TiO_2 into M2 (Ti/c = 0.025) significantly increased the amount of $Ca(OH)_2$ (from 8.6 % in M1 to 10.0 % in M2) and bonded water (from 4.3 % in M1 to 5.7 % in M2), indicating that the hydration reactions were facilitated. With the increase of Ti/c from 0.025 (M2) to 0.1 (M4), the effect was compromised, consistent with the conclusion from the analyses of hydration heat and compressive strength (Fig. 1).

3.2. As(V) removal performance

Single-point tests were conducted to evaluate the As(V) removal performance of these nine mixtures (Fig. 3-A). M1, M2, M3, and M4 were designed to investigate the effect of Ti/c. The As(V) removal decreased from 43 % by M1 to 26 % by M2 (Ti/c of 0.025). The low As(V) removal by M2 might result from the filler effect of nano-TiO_2 particles, which densifies the microstructure and thus partially blocks the penetration of As(V)

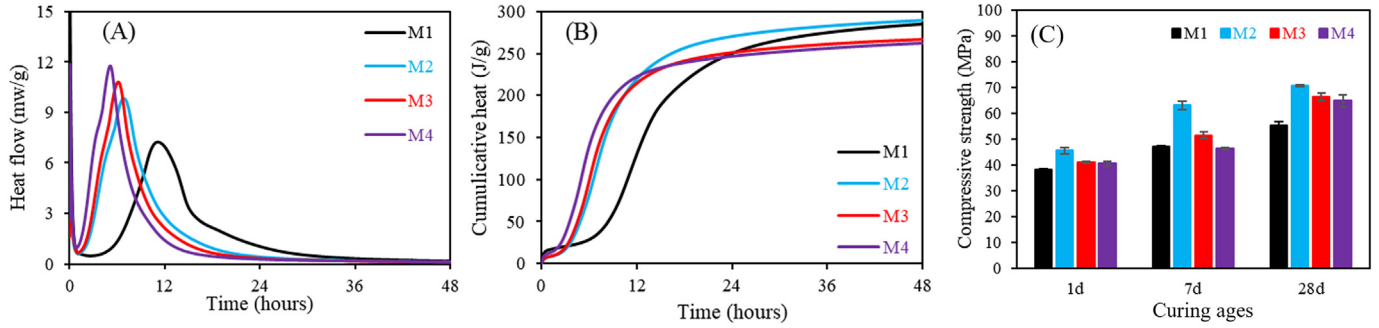

Fig. 1. Heat flow (A) and cumulative heat (B) for the hydration of mixtures with different Ti/c, and the corresponding compressive strength (C) at different curing ages.

solution into the internal TCC (Chen et al., 2012; Meng et al., 2012). However, as the Ti/c increased to 0.05 (M3), the As(V) removal was significantly improved to 57 %, because the TiO_2 content was doubled and the filler effect was compromised, in agreement with the results of hydration heat, compressive strength, and hydration products (Section 3.1). Compared with M3, the Ti/c in M4 (0.1) was doubled but the As(V) removal increased slightly from 57 % to 65 %, indicating that the TiO_2 content might have already reached the limit.

With the increase of w/c from 0.2 of M5 to 0.4 of M3, and to 0.6 of M6, the As(V) removal increased from 8 % by M5 to 26 % by M3, and 62 % by M6, respectively. Therefore, the As(V) removal efficiency was enhanced with the increase of w/c, due to the promoted porosity.

The increase of s/c from 0.5 of M7 to 1 of M3 enhanced the As(V) removal by 14 % (i.e., from 43 % by M7 to 57 % by M3), because of the increased porosity. However, while the s/c reached 1.5 in mixture M8, the As(V) removal was reduced to 43 %, because the excessive sand content in M7 (s/c of 1.5) reduced the percentage of nano-TiO_2, which consequently compromised the As(V) adsorption by TCC.

The replacement of LWS with river sand (50 % by volume) in M9 weakens the As(V) removal from 57 % by M3 to 32 % by M9. This decrease is attributed to more hydration products and reduced porosity of M9 because of the internal curing by LWS (Jiang et al., 2021; Cusson and Hoogeveen, 2008).

Overall, the single-point test indicates that the Ti/c and w/c dominate the As(V) removal. Considering the cost and efficacy, mixtures M3 and M6 were selected for the subsequent studies, and M1 was used as the control.

The kinetic behavior of As(V) adsorption by M1, M3, and M6 was investigated and shown in Fig. 3-B. The adsorbed As(V) increased fast in the first hour and reached equilibrium within 24 h. pseudo-first-order are used to fit these data (Text S2). The fitting results in the linear form are shown in Fig. S5 and Table S4. For these three cases, the data were fitted better by the pseudo-second-order model (R^2 = 0.995–0.999) than the pseudo-first-order model (R^2 = 0.595–0.693), suggesting the rating-limit step for As(V) removal is the chemical adsorption process (Ho and Mckay, 1999). The fitting results showed that the adsorption rate of these three mixtures

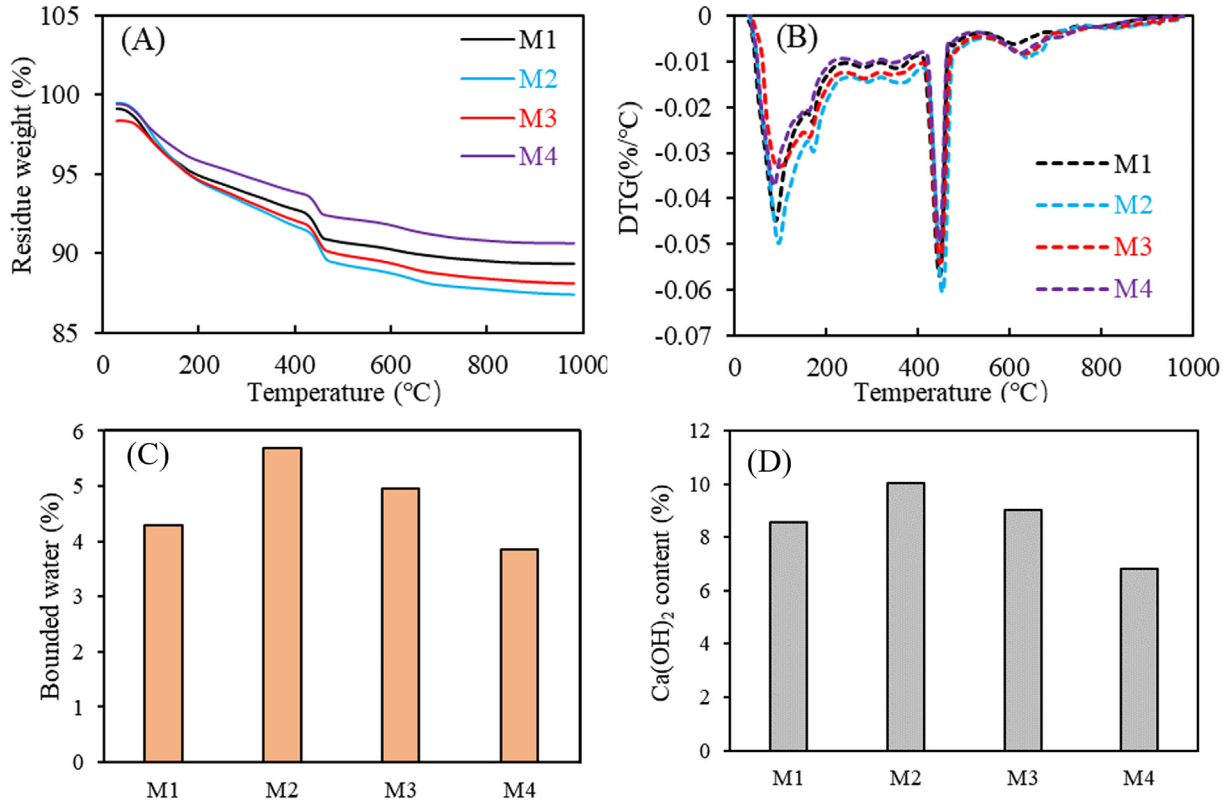

Fig. 2. TGA test results for M1, M2, M3, and M4: (A) the cumulative mass loss, (B) the differential mass loss, (C) the content of bounded water, and (D) the content of $Ca(OH)_2$.

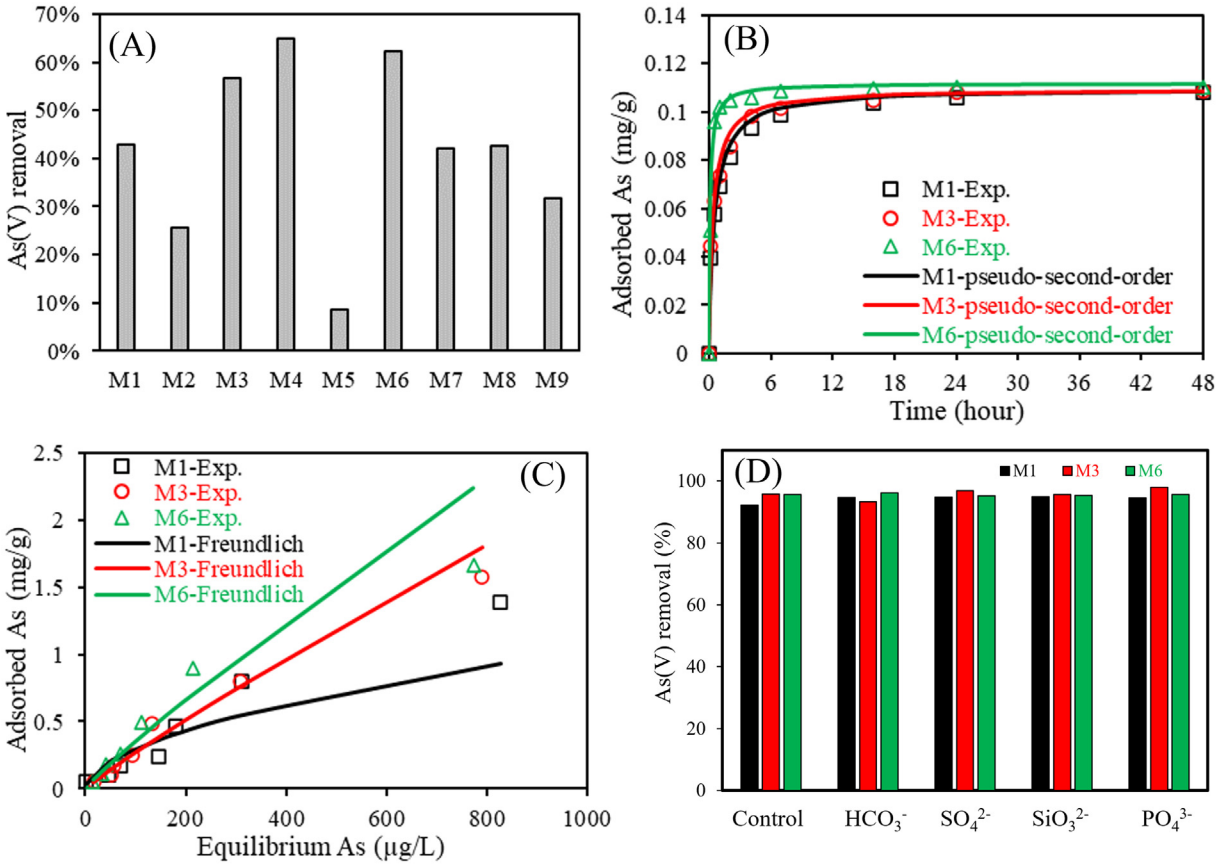

Fig. 3. Single-point test results (A) of nine mixtures (As(V) = 1 mg/L, adsorbent = 1 g/L, adsorption time = 24 h, and equilibrium pH = 6.8–7.2, the data are the average of triplicate tests); kinetic (B) and isotherm (C) study of selected M1, M3, and M6 (As(V) = 1 mg/L; M1, M3, or M6 = 10 g/L; and equilibrium pH = 6.8–7.2); effect of co-existing ions on As(V) removal (As(V) = 1 mg/L; M1, M3, and M6 = 1 g/L; concentrations of PO_4^{3-}, SO_4^{2-}, HCO_3^-, and SiO_3^{2-} are all 1 mg/L; adsorption time = 72 h; and equilibrium pH = 6.8–7.2).

follows the order: M6 (k_2 = 77.8 g mg^{-1} min^{-1}) > M3 (k_2 = 22.2 g mg^{-1} min^{-1}) > M1(k_2 = 16.2 g mg^{-1} min^{-1}).

The isotherms were conducted to investigate the As(V) adsorption capacities of M1, M3, and M6 (Fig. 3-C) and were fitted using Freundlich and Langmuir models (Text S3), which have been widely used for the isotherm model fitting (Kundu and Gupta, 2006b; Naraghi et al., 2018; Afsharnia et al., 2016). The Freundlich model fitted the data better (R^2 = 0.849–0.970, Fig. S6 and Table S5) than the Langmuir model (R^2 = 0.292–0.751), in line with a previous study (Kundu and Gupta, 2006b). Based on the isotherm results, the As(V) adsorption capacities of these three materials follow the order of M6 > M3 > M1, in line with the adsorption rate obtained from the kinetic results (Fig. 3-B).

3.3. Effects of coexisting anions

The effect of coexisting anions (i.e., PO_4, SO_4, HCO_3, and SiO_3) on As(V) removal by M1, M3, and M6 was investigated (Fig. 3-D). Disregarding the presence of these anions, As(V) removal by M1, M3, and M6 was between 93 % and 97 %, indicating that the coexisting anions had an insignificant effect on the As(V) removal. This result agreed well with a previous report (Kundu and Gupta, 2006c), in which the coexisting ions had no noticeable effect on arsenite removal by iron oxides coated cement.

3.4. Reusability analysis

The reusability of TCC for As(V) removal by TCC was evaluated by regeneration tests using 1 M NaOH (Fig. 4). After the first regeneration, the As(V) removal decreased significantly from 92 to 96 % to 57–73 % (Fig. 4-A), and further to 38–55 % in the fourth cycle, indicating an uncompleted regeneration. Notably, in the fourth cycle, the As(V) removal by M3 (55%) and M6 (50%) was much higher than M1 (38%). In addition, the eluted As(V) percentage from M3 (58%, Fig. 4-B) was also higher than the other two types of cementitious composite.

It was reported that As(V) was precipitated with Ca in the cement (Kundu and Gupta, 2008; Jing et al., 2003), while nano-TiO_2 has a high binding affinity to As(V) for the adsorption (Pena et al., 2005; Dutta et al., 2004). Generally, NaOH solution works well for desorbing the adsorbed As(V) but not for precipitated As(V). Therefore, NaOH can desorb the adsorbed As(V) on nano-TiO_2 in M3 and M6 but not for precipitated As(V) in these three mixtures, leading to a higher regeneration ability of M3 and M6 than M1. Overall, the results indicate that the addition of nano-TiO_2 also improves the reusability of cementitious composite for As(V) removal.

3.5. Application in a simulated sewer system

Three opening channels made of M1, M3, and M6 were employed to simulate the real sewer system (Fig. S3). The As(V) concentrations decreased significantly after flowing through the channel (Fig. 5-A). In terms of As(V) removal ability, M3 and M6 were better than M1. In the first 7 h (Fig. 5-B), the effluent As concentrations of the M1 channel is 12–23 μg/L, while these of the M3 and M6 channels are lower than 10 μg/L (the WHO drinking water standard). The effluent As(V) of M3 and M6 channels is still lower (65–73 μg/L) than that of the M1 channel (75 μg/L) until 50 h. Overall, the TCC-sewer (M3 and M6) with a length of 1 m and a diameter of 25.4 mm can treat 0.42 L water containing 100 μg/L As(V) to a safety As(V) level (i.e., < 10 μg/L), while the plain cement cementitious fails. It is important that the incorporation of nano-TiO_2 further

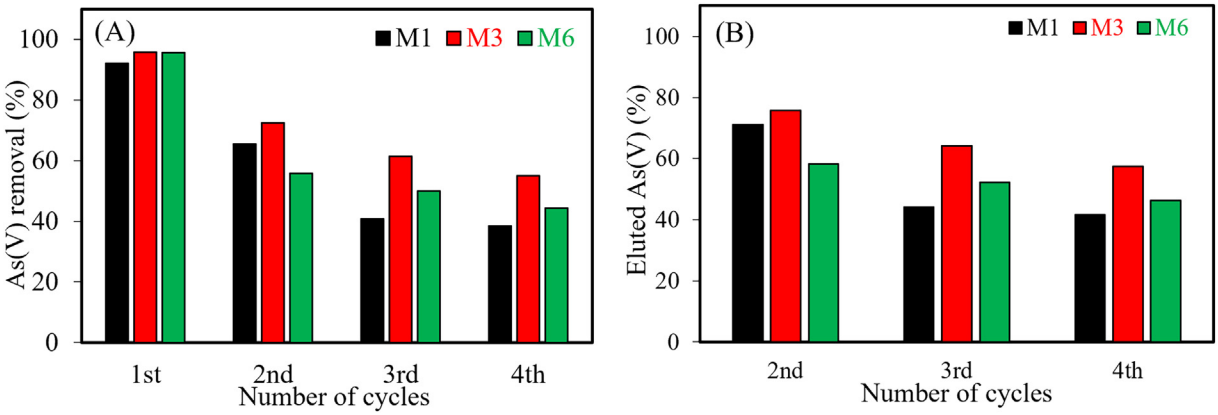

Fig. 4. Regeneration of M1, M3, and M6: (A) As(V) removal and (B) eluted As(V) in each cycle. (As(V) = 1 mg/L; M1, M3, and M6 = 1 g/L; adsorption time = 72 h; desorption time = 1 h, equilibrium pH = 6.8–7.2).

reduces waste water the residual As(V) from 12 to 23 μg/L to 10 μg/L, which might result from the higher adsorption affinity of TiO_2 rather than plain cement cementitious. To further confirm this hypothesis, we further conducted mechanistic study in the following section.

3.6. Mechanistic analysis

The pore size distributions of M1, M3, and M6 (Fig. 6-A) show that the total pore volume of M1 (0.069 mL/g) is higher than M3 (0.045 mL/g) and M6 (0.062 mL/g). The differential pore size distribution (Fig. 6-B) indicates that the pore size of M3 and M6 is smaller than M1. Herein, it can be concluded that the addition of nano-TiO_2 reduced the porosity of the cementitious composite, while the increase of w/c promoted the porosity. With a greater porosity, As(V) solution is easier to penetrate the surface of TCC, thus enhancing the As(V) removal, evidenced by the better removal performance of M6 than that of M3. Therefore, with fixed nano-TiO_2 content, a larger w/c is favored for TCC design in terms of As(V) removal.

To explore the removal mechanisms, samples of M1, M3, and M6 after mixing with 1 and 100 mg/L As(V) solutions were characterized by the extended X-ray absorption fine structure (EXAFS) analysis (Fig. 7 & Table S6). The first Fourier transformed (FT) peaks in R-space for all these samples (Fig. 7-B) are at the same position, which is attributed to four oxygen (O) atoms surrounding As atom with a bond length of 1.69 Å (Table S6). However, while only a second FT peak is observed for M1 samples after mixing 100 mg/L As(V) solution (M1–100 mg/L), an additional FT peak appears for all other five samples.

Specifically, only one second-shell of Ca is found for M1–100 mg/L, which is fitted with 5.9 Ca atoms with an interatomic distance to As(V) (d_{Ca-As}) of ~3.7 Å (Fig. 7-B and Table S6). These values agreed well with the local environment around As(V) in the Ca—As precipitation (i.e., $CaHAsO_4$ (Ferraris and Chiari, 1970), Fig. 7-D), suggesting that the precipitation is the major removal mechanism under this condition. For samples of M3–100 mg/L and M6–100 mg/L, the fitting results reveal an additional shell of 0.2 Ti atoms with d_{Ti-As} of 2.95–3.05 Å. These results imply that partial As(V) might be adsorbed onto TiO_2. However, the low CN of Ti (i.e., 0.2) indicates that the fraction of adsorbed As(V) accounts for ~10 % of totally removed As(V). Therefore, the majority of removed As(V) still exists as precipitated As(V).

For concrete samples mixed with 1 mg/L As(V), the additional FT peak of M1 samples results from 1.8 Ca atoms with a d_{Ca-As} of 2.99 Å. This short d_{Ca-As} is in line with adsorbed As(V) on calcite (Bardelli et al., 2011) (Fig. 7-E), indicating the existence of As(V) adsorbed on calcite or other calcium minerals. Meanwhile, the additional FT peak of M3 and M6 samples are due to 2–2.1 Ti atoms with d_{Ti-As} of ~2.9 Å, suggesting a bidentate mononuclear configuration (Fig. 7-F). Please note, the FT peak resulting from Ca at ~3.6 Å still exists for all these three samples. Hence, the Ca—As precipitation is still involved in 1 mg/L As(V) removal by M1, M3, and M6 samples.

Overall, based on the EXAFS results, the major As(V) removal mechanisms by TCC are the precipitation with Ca and adsorption by nano-TiO_2. The contribution from the adsorption by nano-TiO_2 is more significant when the As(V) concentration is 1 mg/L. This result explains why the improvement of As(V) removal with the incorporation of nano-TiO_2 is more

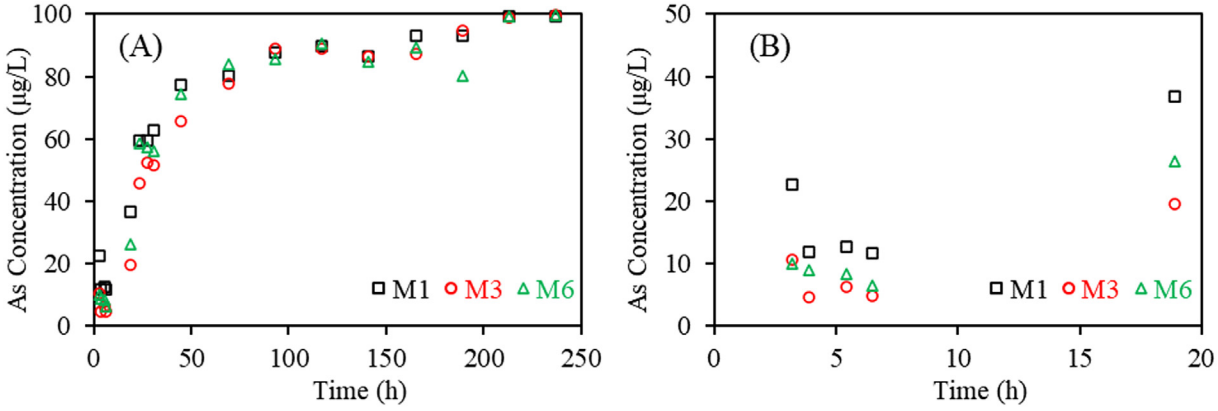

Fig. 5. Effluent As (A) after flowing through in the simulated sewer system (i.e., the flowing channel) made of M1, M3, and M6 (flow rate = 1 mL/min, the length of the channel = 1 m, the diameter of the channel = 25.4 mm, influent As(V) = 100 μg/L). Part B highlights the effluent As in the first 20 h.

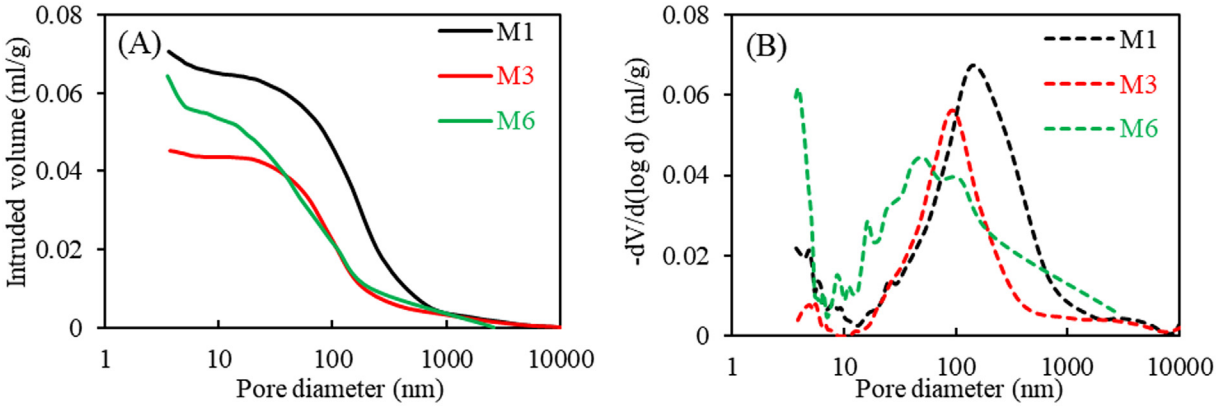

Fig. 6. Pore structure profile identified with MIP: (A) cumulative pore size distribution, and (B) differential pore size distribution.

significant at lower As(V) concentrations, which was observed in the isotherm study (Fig. 3-C).

3.7. Cost analysis

The cost of plain cementitious (M1) and TCC (M3 and M6) are calculated based on the unit cost of the raw materials listed in Table S7 (Jiang et al., 2022; Chiaia et al., 2014; Anonymous, n.d.) and the composition of these three mixtures (Table S8). The calculated cost for M1, M3, and M6 are 61.5, 105.1, and 97.2 USD/ton (Table S9). As stated in Section 3.3, a 1-m long and 2.54-cm diameter sewer made of M3 and M6 can treat 0.42 L wastewater containing 100 μg/L As(V) (i.e., reduce As(V) to <10 μg/L, the WHO standard), while that made of M1 has no such ability. The standard sewer pipe in the US is of 30-in. diameter and 3.75-in. thickness (Astm, 2007), so the 1-m standard sewer pipe can treat 378 L wastewater as it has 900 times contact area with wastewater. Hence, the additional cost for arsenate removal from wastewater by M3 and M6 are 25.8 and 19.2 USD/m^3, respectively. This value is comparable to commercially available adsorptive materials (0–299 USD/m^3 (Shan et al., 2019)). Moreover, there is no additional procedure required for sewer made of TCC to treat municipal wastewater. Therefore, the cost of labor and equipment are nearly zero, while traditional technologies need labor and some set-up to operate. Therefore, this technology is practically useful in terms of As(V) treatment ability and the economic cost.

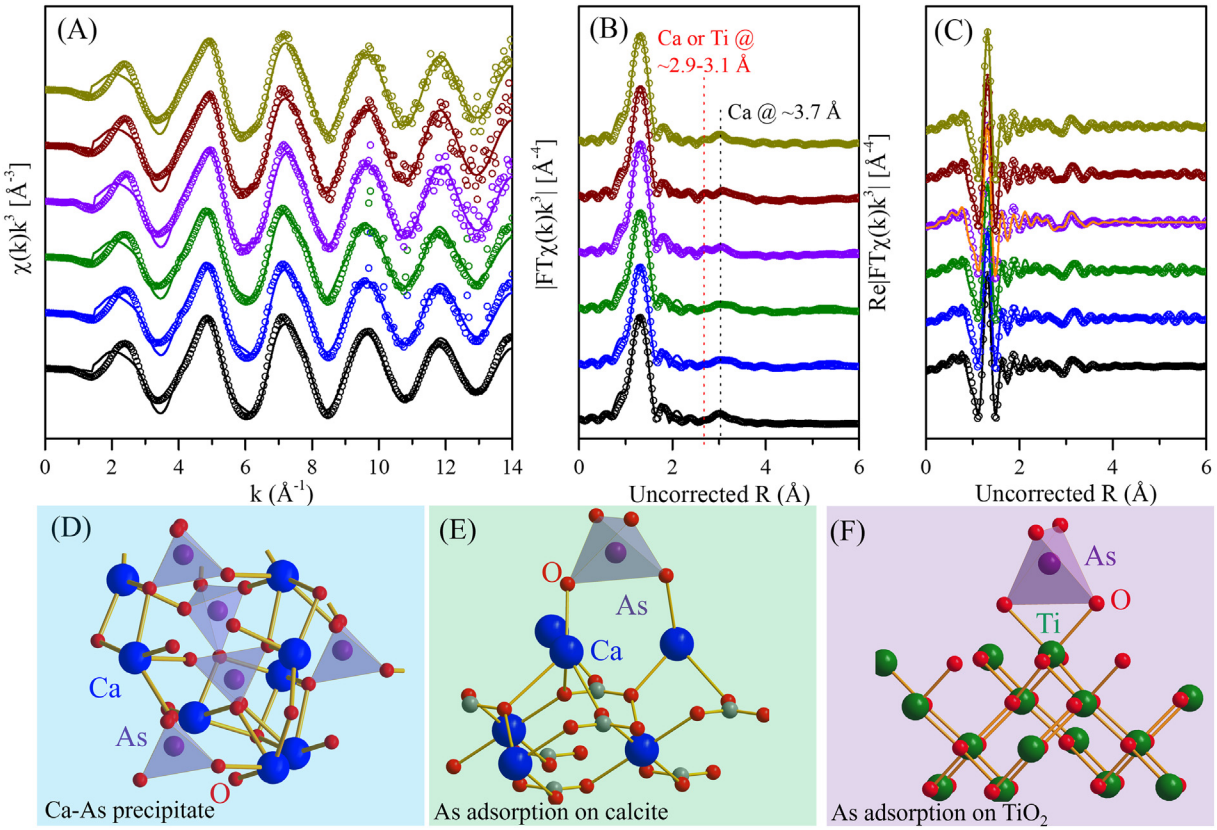

Fig. 7. Normalized k^3-weighted experimental (symbols) and simulated (lines) As K-edge EXAFS for M1, M3, and M6 after mixing with the solutions in the presence of 1 or 100 mg/L (A), the corresponding Fourier transformed magnitude (B) and real parts of Fourier transform (C). The FEFF fitting results are listed in Table S6. Molecular illustration of the Ca—As precipitate (D) and adsorbed As(V) on calcite (E) and TiO_2 (F).

4. Conclusions

This study investigates the effects of using TCC on removing As(V) from wastewater and the underlying mechanisms using EXAFS at the molecular level. The mixture design variables of TCC were evaluated. Flowing channels made using TCC were used to simulate sewer systems for evaluation of the As(V) removal performance.

Based on the investigations, the following conclusions are drawn:

(1) The Ti/c and w/c dominated the As(V) removal performance. The TCC mixture with Ti/c of 0.05 and w/c of 0.6 was the optimum mixture for As(V) removal, which removed 62 % from a 1 mg/L As(V) solution in 24 h.
(2) Sewers fabricated with TCC effectively decontaminated As(V) from flowing water. With the addition of nano-TiO_2, As(V) removal efficiency increased significantly in the first 7 h, where the effluent As(V) was reduced to <10 μg/L.
(3) Precipitation with Ca and adsorption on TiO_2 occurred simultaneously when TCC was used for As(V) removal. Adsorption was more significant when the As(V) concentration was low (i.e., 1 mg/L). Incorporation of nano-TiO_2 promoted As(V) removal.

This study will advance future research on removing As(V) using cementitious composites, especially from municipal wastewater by sewer systems. The revealed mechanisms elucidate the roles of nano-TiO_2 and mixture design variables of TCC, which helps tailor TCC for As(V) and other hazardous oxyanions removal under different conditions.

CRediT authorship contribution statement

Zhuo Liu: Data curation, Formal analysis, Writing – original draft, Writing – review & editing. **Qiantao Shi:** Conceptualization, Investigation, Data curation, Software, Methodology, Formal analysis, Writing – original draft, Writing – review & editing. **Yi Bao:** Conceptualization, Resources, Writing – review & editing. **Xiaoguang Meng:** Resources, Writing – review & editing. **Weina Meng:** Resources, Writing – review & editing.

Data availability

Data will be made available on request.

Declaration of competing interest

The authors declare the following financial interests/personal relationships which may be considered as potential competing interests: Weina Meng reports financial support was provided by National Science Foundation.

Acknowledgments

This research was funded by the National Science and Foundation [award number: CMMI-2046407]. This research used resources of the Advanced Photon Source (APS), a U.S. Department of Energy (DOE) Office of Science User Facility operated for the DOE Office of Science by Argonne National Laboratory under Contract No. DE-AC02-06CH11357. The authors thank Dr. George E. Sterbinsky at 9 BM beamline for his kind help on XAS spectra collection and data analysis. The authors also thank Dr. Tseng-Ming Chou at Stevens Institute of Technology for the help with the SEM-EDS analysis.

Appendix A. Supplementary data

Chemical composition of tap water used in this study and the Type I Portland Cement; Particle size distribution of the river sand; Properties of the nano-TiO_2 used in this study; Photo and illustration of the set-up to simulate the sewer system; Morphology of TiO_2 and TCC, as well as the distribution of Ti element; EXAFS analysis procedure and fitting results; Kinetic and isotherm modeling (PDF). Supplementary data to this article can be found online at https://doi.org/10.1016/j.scitotenv.2022.158754.

References

Abdul, Khaja Shameem Mohammed, Jayasinghe, Sudheera Sammanthi, Chandana, Ediriweera Ps, Jayasumana, Channa, Silva, P.Mangala Cs De, 2015. Arsenic and human health effects: a review. Environ. Toxicol. Pharmacol. 40 (3), 828–846. https://doi.org/10.1016/j.etap.2015.09.016.

Afsharnia, Mojtaba, Saeidi, Mahdi, Zarei, Amin, Narooie, Mohammad Reza, Biglari, Hamed, 2016. Phenol removal from aqueous environment by adsorption onto pomegranate peel carbon. Electron. Physician 8 (11), 3248.

Amini, Manouchehr, Abbaspour, Karim C., Berg, Michael, Winkel, Lenny, Hug, Stephan J., Hoehn, Eduard, Yang, Hong, Johnson, C.Annette, 2008. Statistical modeling of global geogenic arsenic contamination in groundwater. Environ. Sci. Technol. 42 (10), 3669–3675. https://doi.org/10.1021/es702859e.

Andrianisa, Harinaivo Anderson, Ito, Ayumi, Sasaki, Atsushi, Aizawa, Jiro, Umita, Teruyuki, 2008. Biotransformation of arsenic species by activated sludge and removal of bio-oxidised arsenate from wastewater by coagulation with ferric chloride. Water Res. 42 (19), 4809–4817. https://doi.org/10.1016/j.watres.2008.08.027.

Anonymous, .. Available from https://www.alibaba.com/product-detail/20nm-High-Quality-Tio2-Degussa-P25_1600275043366.html?spm=a2700.7724857.0.0.2f516c9ajzMzcl.

Astm, 2007. Standard Specification for Reinforced Concrete Elliptical Culvert, Storm Drain, and Sewer Pipe.

Ayotte, Joseph D., Orcid, Laura Medalie, Qi, Sharon L., Backer, Lorraine C., Nolan, Bernard T., 2017. Estimating the High-Arsenic Domestic-Well Population in the Conterminous United States. Environ. Sci. Technol. 51 (21), 12443–12454. https://doi.org/10.1021/acs.est.7b02881.

Bang, Sunbaek, Pena, Maria E., Patel, Manish, Lippincott, Lee, Meng, Xiaoguang, Kim, Kyoung-Woong, Health, 2011. Removal of arsenate from water by adsorbents: a comparative case study. Environ. Geochem. 33 (1), 133–141.

Bardelli, Fabrizio, Benvenuti, Marco, Costagliola, Pilario, Di Benedetto, Francesco, Lattanzi, Pierfranco, Meneghini, Carlo, Romanelli, Marco, Valenzano, Loredana, 2011. Arsenic uptake by natural calcite: an XAS study. Geochim. Cosmochim. Acta 75 (11), 3011–3023. https://doi.org/10.1016/j.gca.2011.03.003.

Brammer, Hugh, Ravenscroft, Peter, 2009. Arsenic in groundwater: a threat to sustainable agriculture in south and south-East Asia. Environ. Int. 35 (3), 647–654. https://doi.org/10.1016/j.envint.2008.10.004.

Chen, Jun, Kou, Shi-Cong, Poon, Chi-Sun, 2012. Hydration and properties of nano-TiO2 blended cement composites. Cem. Concr. Compos. 34 (5), 642–649. https://doi.org/10.1016/j.cemconcomp.2012.02.009.

Chiaia, Bernardino, Fantilli, Alessandro P., Guerini, Alexandre, Volpatti, Giovanni, Zampini, Davide, 2014. Eco-mechanical index for structural concrete. Construct. Build. Mater. 67, 386–392.

Cusson, Daniel, Hoogeveen, Ted, 2008. Internal curing of high-performance concrete with pre-soaked fine lightweight aggregate for prevention of autogenous shrinkage cracking. Cem. Concr. Res. 38 (6), 757–765. https://doi.org/10.1016/j.cemconres.2008.02.001.

Dutta, Paritam K., Ray, Ajay K., Sharma, Virender K., Millero, Frank J., 2004. Adsorption of arsenate and arsenite on titanium dioxide suspensions. J. Colloid Interface Sci. 278 (2), 270–275. https://doi.org/10.1016/j.jcis.2004.06.015.

Eslami, Hadi, Ehrampoush, Mohammad Hassan, Esmaeili, Abbas, Ebrahimi, Ali Asghar, Salmani, Mohammad Hossein, Ghaneian, Mohammad Taghi, Falahzadeh, Hossein, 2018. Efficient photocatalytic oxidation of arsenite from contaminated water by Fe2O3-Mn2O3 nanocomposite under UVA radiation and process optimization with experimental design. Chemosphere 207, 303–312. https://doi.org/10.1016/j.chemosphere.2018.05.106.

Eslami, Hadi, Ehrampoush, Mohammad Hassan, Esmaeili, Abbas, Salmani, Mohammad Hossein, Ebrahimi, Ali Asghar, Ghaneian, Mohammad Taghi, Falahzadeh, Hossein, Fard, Reza Fouladi, 2019. Enhanced coagulation process by Fe-Mn bimetal nano-oxides in combination with inorganic polymer coagulants for improving As(V) removal from contaminated water. J. Clean. Prod. 208, 384–392. https://doi.org/10.1016/j.jclepro.2018.10.142.

Eslami, Hadi, Esmaeili, Abbas, Ehrampoush, Mohammad Hassan, Ebrahimi, Ali Asghar, Taghavi, Mahmoud, Khosravi, Rasoul, 2020. Simultaneous presence of poly titanium chloride and Fe2O3-Mn2O3 nanocomposite in the enhanced coagulation for high rate As(V) removal from contaminated water. J. Water Process Eng. 36, 101342. https://doi.org/10.1016/j.jwpe.2020.101342.

Eslami, Hadi, Esmaeili, Abbas, Razaeian, Mohsen, Salari, Mahnaz, Hosseini, Abdolreza Nassab, Mobini, Mohammad, Barani, Ali, 2022. Potentially toxic metal concentration, spatial distribution, and health risk assessment in drinking groundwater resources of southeast Iran. Geosci. Front. 13 (1), 101276. https://doi.org/10.1016/j.gsf.2021.101276.

Ferraris, Giovanni, Chiari, Giacomo, 1970. The crystal structure of CaHAsO4 (weilite). Acta Crystallogr. Sect. B 26 (4), 403–410. https://doi.org/10.1107/S0567740870002467.

Ho, Yuh-Shan, Mckay, Gordon, 1999. Pseudo-second order model for sorption processes. Process Biochem. 34 (5), 451–465. https://doi.org/10.1016/S0032-9592(98)00112-5.

Jiang, Du., Meng, Weina, Khayat, Kamal H., Bao, Yi, Guo, Pengwei, Lyu, Zhenghua, Abu-Obeidah, Adi, Nassif, Hani, Wang, Hao, 2021. New development of ultra-high-performance concrete (UHPC). Compos. Part B 224, 109220. https://doi.org/10.1016/j.compositesb.2021.109220.

Jiang, Du., Liu, Zhuo, Christodoulatos, Christos, Conway, Matthew, Bao, Yi, Meng, Weina, 2022. Utilization of off-specification fly ash in preparing ultra-high-performance concrete

(UHPC): mixture design, characterization, and life-cycle assessment. Resour. Conserv. Recycl. 180, 106136.
Jing, Chuanyong, Korfiatis, George P., Meng, Xiaoguang, 2003. Immobilization mechanisms of arsenate in iron hydroxide sludge stabilized with cement. Environ. Sci. Technol. 37 (21), 5050–5056. https://doi.org/10.1021/es021027g.
Jing, Chuanyong, Meng, Xiaoguang, Liu, Suqin, Baidas, Salem, Patraju, Ravi, 2005. Christos christodoulatos and George P korfiatis, surface complexation of organic arsenic on nanocrystalline titanium oxide. J. Colloid Interface Sci. 290 (1), 14–21.
Kundu, Sanghamitra, Gupta, Ashok Kumar, 2006. Arsenic adsorption onto iron oxide-coated cement (IOCC): Regression analysis of equilibrium data with several isotherm models and their optimization. Chem. Eng. J. 122 (1), 93–106. https://doi.org/10.1016/j.cej.2006.06.002.
Kundu, Sanghamitra, Gupta, Ak, 2006. Arsenic adsorption onto iron oxide-coated cement (IOCC): regression analysis of equilibrium data with several isotherm models and their optimization. Chem. Eng. J. 122 (1–2), 93–106.
Kundu, Sanghamitra, Gupta, A.K., 2006. Adsorptive removal of As(III) from aqueous solution using iron oxide coated cement (IOCC): evaluation of kinetic, equilibrium and thermodynamic models. Sep. Purif. Technol. 51 (2), 165–172. https://doi.org/10.1016/j.seppur.2006.01.007.
Kundu, Sanghamitra, Gupta, A.K., 2008. Immobilization and leaching characteristics of arsenic from cement and/or lime solidified/stabilized spent adsorbent containing arsenic. J. Hazard. Mater. 153 (1), 434–443. https://doi.org/10.1016/j.jhazmat.2007.08.073.
Kundu, Subrata, Kavalakatt, Shaunpaul Simon, Pal, Anjali, Ghosh, Sujit Kumar, Mandal, Madhuri, Pal, Tarasankar, 2004. Removal of arsenic using hardened paste of Portland cement: batch adsorption and column study. Water Res. 38 (17), 3780–3790.
Meng, Tao, Yachao, Yu., Qian, Xiaoqian, Zhan, Shulin, Qian, Kuangliang, 2012. Effect of nano-TiO2 on the mechanical properties of cement mortar. Constr. Build. Mater. 29, 241–245. https://doi.org/10.1016/j.conbuildmat.2011.10.047.
Naraghi, Behnaz, Baneshi, Mohammad Mehdi, Amiri, Reza, Dorost, Amin, Biglari, Hamed, 2018. Removal of Reactive Black 5 dye from aqueous solutions by coupled electrocoagulation and bio-adsorbent process. Electron. Physician 10 (7), 7086.
Newville, Matthew, 2001. IFEFFIT: interactive XAFS analysis and FEFF fitting. J. Synchrotron Radiat. 8, 322–324. https://doi.org/10.1107/S0909049500016964.
Pena, Maria E., Korfiatis, George P., Patel, Manish, Lippincott, Lee, Meng, Xiaoguang, 2005. Adsorption of As(V) and As(III) by nanocrystalline titanium dioxide. Water Res. 39 (11), 2327–2337. https://doi.org/10.1016/j.watres.2005.04.006.
Podgorski, Joel, Berg, Michael, 2020. Global threat of arsenic in groundwater. Science 368 (6493), 845–850. https://doi.org/10.1126/science.aba1510.
Qin, Ling, Gao, Xiaojian, Li, Qiyan, 2018. Upcycling carbon dioxide to improve mechanical strength of Portland cement. J. Clean. Prod. 196, 726–738. https://doi.org/10.1016/j.jclepro.2018.06.120.
Ravel, Bruce, Newville, Matthew, 2005. ATHENA, ARTEMIS, HEPHAESTUS: data analysis for X-ray absorption spectroscopy using IFEFFIT. J. Synchrotron Radiat. 12, 537–541. https://doi.org/10.1107/S0909049505012719.
Shan, Yina, Mehta, Praem, Perera, Duminda, Varela, Yurissa, 2019. Cost and Efficiency of Arsenic Removal From Groundwater: A Review. United Nations University-Institute for Water, Environment and Health Hamilton.
Shi, Qiantao, Zhang, Shujuan, Ge, Jie, Wei, Jinshan, Christodoulatos, Christos, Korfiatis, George P., Meng, Xiaoguang, 2020. Lead immobilization by phosphate in the presence of iron oxides: adsorption versus precipitation. Water Res. 179, 115853. https://doi.org/10.1016/j.watres.2020.115853.
Singh, Rachana, Singh, Samiksha, Parihar, Parul, 2015. Vijay pratap Singh and Sheo Mohan prasad, arsenic contamination, consequences and remediation techniques: a review. Ecotoxicol. Environ. Saf. 112, 247–270. https://doi.org/10.1016/j.ecoenv.2014.10.009.
Zhai, Weiwei, Qin, Tianyue, Li, Liguan, Guo, Ting, Yin, Xiaole, Khan, Muhammad Imran, Hashmi, Muhammad Zaffar, Liu, Xingmei, Tang, Xianjin, Xu, Jianming, 2020. Abundance and diversity of microbial arsenic biotransformation genes in the sludge of full-scale anaerobic digesters from a municipal wastewater treatment plant. Environ. Int. 138, 105535. https://doi.org/10.1016/j.envint.2020.105535.
Zhang, Shujuan, Shi, Qiantao, Chou, Tseng-Ming, Christodoulatos, Christos, Korfiatis, George P., Meng, Xiaoguang, 2020. Mechanistic study of Pb(II) removal by TiO2 and effect of PO4. Langmuir 36 (46), 13918–13927. https://doi.org/10.1021/acs.langmuir.0c02388.
Zhenhai, Xu., Zhou, Zonghui, Peng, Du., Cheng, Xin, 2017. Effects of nano-limestone on hydration properties of tricalcium silicate. J. Therm. Anal. Calorim. 129 (1), 75–83. https://doi.org/10.1007/s10973-017-6123-9.